PERGAMON

International Journal of Multiphase Flow 28 (2002) 1437–1457

International Journal of Multiphase Flow

www.elsevier.com/locate/ijmulflow

Spreading of an axisymmetric viscous drop due to gravity and capillarity on a dry horizontal wall

S.N. Reznik, A.L. Yarin *

Faculty of Mechanical Engineering, Technion—Israel Institute of Technology, Haifa 32000, Israel

Received 25 November 2001; received in revised form 3 June 2002

Abstract

Spreading of an axisymmetrical drop on a dry plane horizontal wall under the action of gravity and surface tension (or capillarity) is studied in the inertialess approximation for arbitrary Bond numbers. It is shown that the initial stage of spreading is completely dominated by gravity, and rolling motion sets in at the contact line (CL). When the rate of the CL motion reduces to the order of the characteristic wetting velocity expected from the Hoffman's well-known law, wetting effects begin to play an important role. However, the apparent contact angle at this stage is still affected by the bulk flow and only at its end approaches Hoffman's law. Deviations from the latter are shown to be important in the region of contact angles close to π and to increase with the Bond number, owing the fact that the bulk flow effects driven by gravity are stronger, the higher the Bond number. Accordingly the apparent contact angle increases with the Bond number, which is in qualitative agreement with experimental observations. Comparison with known analytical solutions is presented.

Keywords: Drop spreading; Moving contact line; Apparent contact angle; Bulk flow effect

1. Introduction

The theme of the present work is spreading of the axisymmetrical drops on a plane horizontal dry wall. This problem has been considered in literature in different contexts. For example, in the case of drop impact with impact velocity sufficiently high and significant inertial forces, splashing, jetting, bubble encapsulation, and capillary wave propagation are encountered, especially in the case of a wet surface (Yarin and Weiss, 1995; Weiss and Yarin, 1999; Gueyffier and Zaleski, 1998; Rieber and Frohm, 1999). In the present work, however, we deal with the situation where inertial

* Corresponding author.
E-mail address: meralya@yarin.technion.ac.il (A.L. Yarin).

0301-9322/02/$ - see front matter
PII: S0301-9322(02)00043-5

effects are negligible and spreading proceeds in a creeping flow regime due to gravity. Such flows have recently attracted considerable attention in literature due to their technological importance (Chandra and Avedisian, 1991; Gao and Sonin, 1994; Fukai et al., 1993, 1995; Hatta et al., 1995; Pasandideh-Fard et al., 1996; Schiaffino and Sonin, 1997a,b; Waldvogel and Poulikakos, 1997; Davidson, 2000), but the physical processes affecting the dynamics of propagation of the moving contact line (CL) (the drop edge) over a dry surface, especially interplay between wettability and bulk flow effects, have not yet been adequately treated. The present work deals with this aspect.

A number of publications, both experimental and theoretical, suggest that in a creeping flow regime the apparent dynamic contact angle is determined by the motion rate of the CL, the viscosity of the liquid, surface tension, and such molecular factors as the London–van der Waals forces significant in the vicinity of the CL (de Gennes, 1985). Hoffman's experiments (Hoffman, 1975) yielded a nearly universal relation between the rate of motion of the CL, the apparent contact angle and the equilibrium contact angle for wetting over a wide range of CL motion rates. Cox (1986) showed that the law has a universal form but contains a term depending on the flow at some distance from the CL. This term was calculated analytically in Hocking (1983) in the framework of the lubrication approximation for the case of drop spreading by gravity and capillarity but only for small apparent contact angles (i.e. at the long-term limit). The results demonstrated that the law of CL motion is close to Hoffman's law for small and moderate Bond numbers. However, the CL motion in the case of large Bond numbers corresponding to strong gravity forcing is affected by the bulk flow resulting from gravity. Analysis of drop spreading with arbitrary apparent contact angles (Hocking and Rivers, 1982) was confined to the case of small drops where gravity effects are negligible.

Modeling of molecular mechanisms near the CL in studies of partial wetting (Thompson and Robbins, 1989; de Gennes et al., 1990) suggests that the microscopic (actual) contact angle is unaffected by the flow in the range of several angstroms and is always determined by Young's relation. This implies that the actual contact angle is a material property of the system, as was postulated in Ngan and Dussan (1982).

At intermediate distances of the order of 1 nm to 100 μm the apparent contact angle is already affected by viscous effects and surface tension. The latter change the slope of the free surface, which results in a difference between the actual microscopic angle and the apparent one seen in the photographs. Since these viscous and surface tension effects are still localized near the moving CL, they result in a universal dependence between its velocity and the apparent and equilibrium contact angles found in Hoffman (1975), Cox (1986), de Gennes et al. (1990). Experiments (Fermigier and Jenffer, 1991) fully supported the universal relation of Cox (1986) in the case of liquid–air interfaces, which is of primary interest in the present work. The relation has been shown to be valid almost up to apparent contact angles close to π and sufficiently high flow velocities—in spite of the fact that for contact angles close to π the CL becomes unstable, and the accuracy of the angle measurements is not too high. Thus Cox's relation can be considered as plausible even for the apparent contact angles close to π, and deviations from it are almost certainly attributable to the effect of roughness (Fermigier and Jenffer, 1991; Zhou and Sheng, 1990). Besides the purely hydrodynamic phenomena near the moving CL treated in Cox (1986), the local molecular-kinetic effects can also contribute to the dependence of the contact angle on the rate of propagation of the CL (cf. Blake (1993) and references therein). In fact, probably both mechanisms contribute, and both theories describe the CL propagation equally well (Hayes and Ralston, 1993).

Strong bulk flow apart from the moving CL necessarily affects the shape of the free surface. This leads to narrowing of the validity range of the universal results found in Hoffman (1975), Cox (1986), which continue to be valid near the CL but in closer and closer proximity as the flow becomes stronger. At the same time, the apparent contact angle becomes dependent on the intensity and geometry of the bulk flow as a whole, as is actually suggested by the results of Hocking (1983), Ngan and Dussan (1982), Hayes and Ralston (1993), as well as by those of the present work. In it we consider a drop spreading on a plane dry horizontal wall for arbitrary values of the Bond number, including those corresponding to strong gravity forcing (in the creeping flow approximation), without any restrictions on the apparent contact angle. One of the main aspects treated is the dynamics of the moving CL during the spreading process. The corresponding study of the present group (Reznik and Yarin, 2002) dealt with planar two-dimensional drops. The present work is devoted to the axisymmetric case.

In Section 2 the problem is formulated. Non-dimensionalization is introduced in Section 3. The case of the moderate Bond numbers is considered in Section 4, and that of large Bond numbers in Section 5. Conclusions are drawn in Section 6.

2. Problem formulation

Consider a spherical drop of viscous liquid placed on a plane horizontal surface at a point O and spreading on it with zero initial velocity (Fig. 1). Denote the surface tension σ and the viscosity μ, and take as their characteristic values $\sigma \sim 100$ g/s^2 and $\mu = 10$ g/cm s. As an estimate of the liquid density, we take $\rho = 1$–10 g/cm^3. The characteristic values are typical of water–glycerine mixtures and solder. The volume-equivalent radius of the drop is set at $a_0 \leqslant 0.1$ cm. A plausible estimate of the characteristic flow velocity is given by the ratio $V = \sigma/\mu$, the corresponding Reynolds number being

$$Re = \frac{\rho V a_0}{\mu} \leqslant 0.1\text{–}1. \tag{1}$$

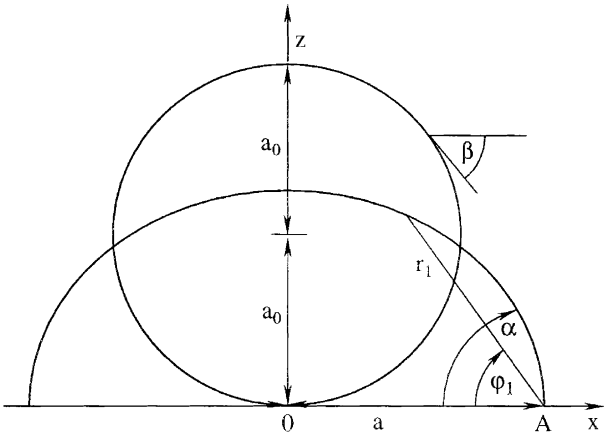

Fig. 1. Sketch of a drop spreading on a horizontal surface.

The Bond number determines the relative importance of the gravity and capillarity effects

$$Bo = \frac{\rho g a_0^2}{\sigma} \sim 0.1\text{–}1, \tag{2}$$

where g is the gravity acceleration.

The values of the Reynolds and the Bond numbers in (1) and (2) are characteristic of small droplets with an intermediate viscosity.

In the Navier–Stokes equations rendered dimensionless using the scales V and a_0, the inertial terms are of order one, the viscous terms are of order Re^{-1}, and the gravitational term is of order Fr^{-1}, where the Froude number $Fr = V^2/(ga_0)$. In the limit of $Re \sim Fr \ll 1$ the inertial terms can be neglected compared to the viscous and gravitational ones. The Reynolds and Froude numbers are of the same order if $V = \sigma/\mu \sim \rho g a_0^2/\mu$. The latter is true for small droplets for the Bond number values of Eq. (2). Therefore in this case the inertial terms are negligibly small and we are dealing with the creeping flow affected by gravity.

Some experiments, however, are conducted with much larger drops of such highly viscous liquids as polydimethylsiloxanes (Marino et al., 1996). In this case $\sigma \simeq 20$ g/s^2, $\mu \simeq 100$–1000 g/(cm s), $\rho \simeq 1$ g/cm^3 and a_0 is from the range of 3.5–7.3 cm. In this case $Bo \geqslant 10^3$ (or even 10^5). In this case the velocity scale $V = \rho g a_0^2/\mu$ yields $Re \sim Fr$ (however, now $V > \sigma/\mu$, since $Bo > 1$). The Reynolds number Re based on this scale $Re = \rho^2 a_0^3 g/\mu^2$ still yields $Re = 10^{-3}$–10^{-1} for the polydimethylsiloxane drops. Therefore in this case we are still dealing with the creeping flow affected by gravity.

In the creeping flow regime we are dealing with, the Stokes equations read

$$\nabla p = \mu \triangle \mathbf{u} + \rho \mathbf{g}, \tag{3}$$

$$\nabla \cdot \mathbf{u} = 0. \tag{4}$$

Here p is the pressure, and $\mathbf{u}$ is the velocity vector. Gravity acceleration $\mathbf{g}$ is directed against the z-axis in Fig. 1.

Due to the drop symmetry about the vertical axis z, intersecting the plate surface at point O (see sketch in Fig. 1), the velocity vector has a radial (r) and a vertical (z) component. The no-slip boundary conditions on a horizontal plane $z = 0$ read

$$u_r = 0, \quad u_z = 0, \quad z = 0. \tag{5}$$

These conditions are valid everywhere except for a small domain of the CL, where intermolecular forces become significant (de Gennes, 1985). When the conditions (5) were also applied at the CL, a force singularity emerged (Dussan and Davis, 1974; Dussan, 1979). To eliminate this singularity, the slip Navier–Maxwell boundary condition was used instead of (5) in Hocking (1983), Hocking and Rivers (1982), Zhou and Sheng (1990), Chen et al. (1996). In the present case the slip condition reads

$$u_r - \bar{\lambda}\frac{\partial u_r}{\partial z} = 0, \quad z = 0 \text{ (near the CL)}. \tag{6}$$

Here $\bar{\lambda}$ is a molecular slip coefficient, which is small relative to the macroscopic scales of the problem (the latter being of the order of a_0).

Cox (1986) (cf. also Hocking and Rivers (1982)), having removed the singularity by condition (6), arrived at the relation for the apparent contact angle discussed in Section 1. He also calculated the flow field in the "hydrodynamic" region adjacent to the CL. His results for the apparent contact angle and the flow field were compared with experiment in Chen et al. (1996). It was shown that the predictions for the flow field fail at distances of the order of 10^2 μm from the moving CL. Also when the flow velocity becomes sufficiently high, the prediction for the apparent contact angle fails.

According to Cox (1986), the law governing the CL motion need not be confined to the particular molecular model used in the vicinity of the CL; this enables us to use (6) safely in the model of the present work.

With the drop shape described by a function $r = h(z,t)$ the kinematic boundary condition at the drop surface reads

$$\frac{\partial h}{\partial t} + u_z \frac{\partial h}{\partial z} = u_r, \quad r = h(z,t), \quad 0 < z < z_a(t), \tag{7}$$

where $z_a(t)$ is the apex coordinate. Note that by setting $r = h(z,t)$ for the drop shape, we are capable of description of only the shapes corresponding to single valued functions r. If in the course of calculations drop shape would tend to "overturn" leading to a multivalued function, r should be parametrized by the arc length of the drop generatrix s. Such cases, however, were not encountered in the present work. Note, that below we also use $r = h(s,t)$, but still as a single valued function.

The dynamic boundary conditions on the drop surface consist as usual in vanishing of the tangential stresses and normal stress balance, with the effect of surface tension included

$$\mathbf{f} \cdot \boldsymbol{\tau} = 0, \quad r = h(z,t), \tag{8}$$

$$\mathbf{f} \cdot \mathbf{n} = \sigma\kappa, \quad r = h(z,t). \tag{9}$$

Here $\mathbf{f}$ is the force acting in the liquid; $\mathbf{n}$ and τ are the unit normal and tangent vectors at the surface; κ is the surface curvature. The latter can be expressed in terms of the slope angle of the surface β, as per

$$\kappa = \frac{1}{r} \frac{\mathrm{d}(r \sin\beta)}{\mathrm{d}r}. \tag{10}$$

($\beta < 0$ is the angle which the tangent to the surface makes with the r-axis; see Fig. 1). The geometrical relation

$$\frac{\mathrm{d}h}{\mathrm{d}z} = \frac{1}{\tan\beta} \tag{11}$$

states the dependence of h on β.

The condition of volume conservation in the axisymmetric case we are dealing with can be expressed in the form

$$2\pi \int_0^{s_{\mathrm{CL}}} hz\cos(\beta)\,\mathrm{d}s = \frac{4\pi}{3} a_0^3, \tag{12}$$

where s is the arc length measured from the apex to the fixed point on a drop generatrix and s_{CL} is its value for point A, corresponding to the CL (see Fig. 1).

The condition at the apex reads

$$\beta = 0, \quad z = z_a. \tag{13}$$

In close proximity to the CL the slope angle should equal its stationary value α_s, determined solely by the intermolecular forces (Hocking and Rivers, 1982; Thompson and Robbins, 1989; de Gennes et al., 1990) (cf. the discussion in Section 1). Thus, the boundary condition at the CL becomes

$$\beta = -\alpha_s, \quad z = 0. \tag{14}$$

The initial shape of the drop generatrix is assumed to be circular

$$h = \sqrt{a_0^2 - (z - a_0)^2}, \quad 0 < z < 2a_0, \quad t = 0. \tag{15}$$

3. Dimensionless parameters

The parameters involved are rendered dimensionless as follows:

$$(r', z', s') = \frac{(r, z, s)}{a_0}, \quad t' = \frac{\sigma t}{\mu a_0}, \quad \lambda = \frac{\bar{\lambda}}{a_0}, \quad h' = \frac{h}{a_0}, \tag{16}$$

$$(u_r', u_z') = \frac{\mu(u_r, u_z)}{\sigma}, \quad p' = \frac{a_0 p}{\sigma}. \tag{17}$$

Eq. (3) in dimensionless form reads (here and hereinafter primes are dropped for brevity)

$$\nabla p = \triangle \mathbf{u} - Bo\mathbf{j} \tag{18}$$

(**j** being the unit vertical vector), whereas the dynamic boundary conditions become

$$\mathbf{f} \cdot \mathbf{n} = \kappa, \quad r = h(z, t), \tag{19}$$

$$\mathbf{f} \cdot \boldsymbol{\tau} = 0, \quad r = h(z, t). \tag{20}$$

The dimensionless kinematic boundary condition at the drop surface is still given by (7), and the initial condition, and that of volume conservation, become

$$h = \sqrt{1 - (z - 1)^2}, \quad 0 < z < 2, \quad t = 0, \tag{21}$$

$$\int_0^{s_{CL}} hz \cos(\beta)\, \mathrm{d}s = \frac{2}{3}. \tag{22}$$

The capillary number based on the CL motion rate U, is defined as per

$$Ca = \frac{\mu U}{\sigma} = \frac{\mathrm{d}a}{\mathrm{d}t}, \tag{23}$$

a being the apparent coordinate of the CL; $a = h(0, t)$ for $t > 0$.

4. Moderate Bond numbers

4.1. From a single-point contact angle to a finite contact area

Calculation of the drop shapes at moderate values of the Bond number began with a circular shape of the drop generatrix. In the time interval $0 \leq t \leqslant t_1$ ($t_1 \leqslant t_*$) the drop progresses from a single-point contact with the wall to a finite contact area (t_* denoting the moment when rolling motion ceases at the CL; see below for details). This stage is completely dominated by the gravity force and inertia, and it can be shown that it is very short even compared to t_*. Indeed, denote by ϕ the semi-angle between the two radii in the median cross-section SS' of the drop such that they end at the points where the CL intersects SS'. At $t = 0$ $\phi = 0$, and at $0 \leqslant t \leqslant t_1$ $\phi \ll 1$. To the value ϕ of the angle corresponds a downward shift of the drop center by $H = a_0(1 - \cos\phi) \simeq a_0\phi^2/2$, and the attendant decrease in the potential energy of the drop E_p is $\rho(4/3)\pi a_0^3 g\,\mathrm{d}H/\mathrm{d}t$. Since, as can be shown the gravity effects outweigh the viscous ones as well as that of surface tension, E_p should equal the sideways flux of the kinetic energy existing near the bottom, $E_k = (\rho v^2/2)2\pi avH$, where v is the characteristic velocity of the flow in this region. The energy balance reads

$$\rho\frac{2}{3}\pi a_0^4 g\frac{\mathrm{d}\phi^2}{\mathrm{d}t} = \frac{\rho v^3 \pi a_0 a}{2}\phi^2. \tag{24}$$

The current position of the CL is $a = a_0\sin\phi \simeq a_0\phi$. Therefore $v = \mathrm{d}a/\mathrm{d}t \simeq a_0\mathrm{d}\phi/\mathrm{d}t$, and Eq. (24) yields

$$\phi = \left(\frac{32}{3}\frac{g}{a_0}\right)^{1/4} t^{1/2}, \tag{25}$$

$$a = a_0\left(\frac{32}{3}\frac{g}{a_0}\right)^{1/4} t^{1/2}. \tag{26}$$

Let us now estimate the time t_1 needed to reach the value of $a = a_1 = 10^{-1}a_0$ for $a_0 = 10^{-1}$ cm. From Eq. (26), $t_1 = (a_1/a_0)^2(32g/3a_0)^{-1/2} = 3 \times 10^{-5}$ s, much smaller than t_*. Indeed, according to Fig. 2 discussed below, $t_* > \mu a_0/\sigma$. For $\mu = 10$ g/cm s, $\sigma = 10^2$ g/s^2 and $a_0 = 10^{-1}$ cm, $t_* > 10^{-2}$ s. Since $t_1 \ll t_*$, we can take $t_1 = 0$ in the calculations.

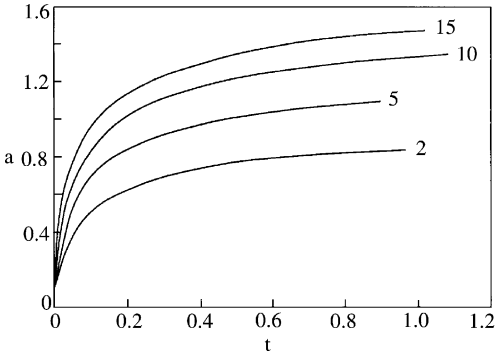

Fig. 2. Position of the moving CL as a function of time during the transition stage of the process. The values of the Bond number are shown by the numerals near the curves.

4.2. The initial transition stage of the spreading

We consider droplet evolution after a finite contact area has already been established. The case of moderate Bond numbers is treated, and at the initial transition stage of spreading the time interval $0 \leqslant t \leqslant t_*$ is covered. It is clear that in this transition process the gravity effects play a dominant role and capillary number is large. In the experiments of Hoffman (1975), contact angle was found to be very close to π for $Ca \geqslant 0.2$. For such values of Ca rolling motion is realized at the CL. At the stage where gravity dominates the flow and Ca is large, evolution of the free surface towards rolling is virtually unaffected by the wettability effects and the latter could be dispensed with. In the present work it was found that this leads to a much more effective numerical algorithm. Note also that, as was shown in Dussan and Davis (1974), there is no singularity in the stresses at the CL when the no-slip boundary condition (5) is applied at $z = 0$ as rolling motion sets in. Then, applying the dynamic boundary conditions (19) and (20), we can obtain the solution of the Stokes Equation (18), using boundary element method (BEM), and determine the flow velocity $\mathbf{u}$ at an arbitrary point of the drop surface. The evolution pattern of the surface generatrix can be found from the equation

$$\frac{\mathrm{d}\mathbf{r}_i}{\mathrm{d}t} = \mathbf{u}(\mathbf{r}_i), \tag{27}$$

where $\mathbf{r}_i$ is the radius vector of the i-th material point at the surface generatrix at time t.

The initial condition for (27) is given by

$$\mathbf{r}_i(0) = \mathbf{r}_i^0, \tag{28}$$

where $\mathbf{r}_i^0$ is the initial coordinate of this point on the circle at $t = 0$.

To solve Eq. (27), we need the velocity $\mathbf{u}$ at the drop surface at $t = 0$. In order to obtain it via BEM, the initial condition was set in the form of a circle with the CL position $a_1 \ll a_0$ at $t = t_1$ as per Eq. (26).

Eq. (27) under the initial condition (28) was integrated by the Kutta–Merson method. At each time step the nodes on the free surface were redistributed, with all those which had moved to the wall discarded. Then new contact line position was determined as the intersection between the surface and the wall, and the new nodes were distributed for the next time step.

The numerically calculated position and motion rate of the CL, as well as capillary number Ca, for $Bo = 2$, 5, 10 and 15 are presented in Figs. 2 and 3. The evolution of the drop surface for these moderate values of Bo is illustrated in Fig. 4. In Fig. 3 it is seen that the motion rate at this transition stage rapidly decreases with time. Eventually it approaches the value of the order of $\mathrm{O}(\epsilon)$; in the present calculations $\epsilon = 0.01$ (which is characteristic of most of the surfaces (de Gennes, 1985)). From Eq. (58) below it is seen that at $\alpha \leqslant 3$, $Ca = \mathrm{O}(\epsilon)$ which means that the wetting velocity is of the order of ϵ. During the transition stage the motion rate of the CL is much higher than the wetting velocity (Fig. 3), however, at the end of this stage at $t = t_*$, the CL velocity inevitably reduces to the level of the wetting velocity. This corresponds to significantly squeezed drop shapes, when gravity effect has already been diminished. An overlap of the initial transition stage of spreading treated in the present subsection with the wetting stage considered below in Section 4.3 takes place at t close to t_*.

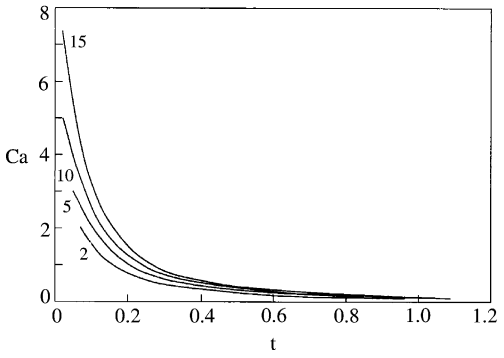

Fig. 3. Capillary number based on the motion rate of the CL as a function of time during the transition stage of the process. The values of the Bond number are shown by the numerals near the curves.

In Fig. 4 it is seen that at the initial transition stage $0 \leqslant t \leqslant t_*$, where $t_* = \mathrm{O}(1)$, the evolution of the drop surface from the initial circular shape (21) is totally governed by the bulk flow driven by gravity, and rolling motion sets in at the CL. In Fig. 4(a) the rolling motion at the CL sets in at $t = 0.0005$, in Fig. 4(b)—$t = 0.0002$, in Fig. 4(c)—$t = 0.0001$, and in Fig. 4(d)—$t = 0.000075$. Effect of surface roughness should be negligible at this stage. Only at $t > t_*$ do the molecular wetting effects become competitive and the quasi-stationary scenario studied earlier in Hocking and Rivers (1982) sets in. The time delay $t_* = \mathrm{O}(1)$ before this takes place increases with the Bond number, as gravity squeezing becomes more intensive. The value of t_* can be estimated using the fact that at the transition stage of droplet motion the surface tension plays only a minor role and the dependence of the CL coordinate on time satisfies the same equation as for the large Bond numbers (Eq. (65) below in Section 5). From this equation we can find $t_* \sim (Bo/(6\epsilon)^8)^{1/7}$. Then for $\epsilon \sim 0.01$ the value of t_* increases from 27.5 to 36.7 as the Bond number increases from $Bo = 2$ to 15. The dimensional time corresponding to $t_* = \mathrm{O}(1)$ is $t = \mathrm{O}(\mu a_0/\sigma)$.

The evolution of the apparent contact angle towards the value of $\alpha = \pi$, and the appearence of rolling motion at the CL found in the present work agree with the experimental evidence of Marino et al. (1996). Note also that gravity-driven spreading of viscous drops was studied numerically in Betelu et al. (1997). There are two main differences between the latter work and the present one. First, the variant of the BEM employed in Betelu et al. (1997) does not allow for an easy incorporation of the surface tension. Therefore they considered only the case of $\sigma = 0$. Second, Betelu et al. (1997) did not allow for a free evolution of the apparent contact angle, as in the present work, but postulated rolling motion at the CL ($\alpha = \pi$) from the very beginning.

4.3. Calculation of the drop shape at the wetting stage

At $t > t_*$ wettability effects become important. In Hocking and Rivers (1982) it was assumed that for moderate and small Bond numbers, where the gravity effects are relatively small, the capillary number is as small as in the case $Bo = 0$. The law of the CL motion can then be found via

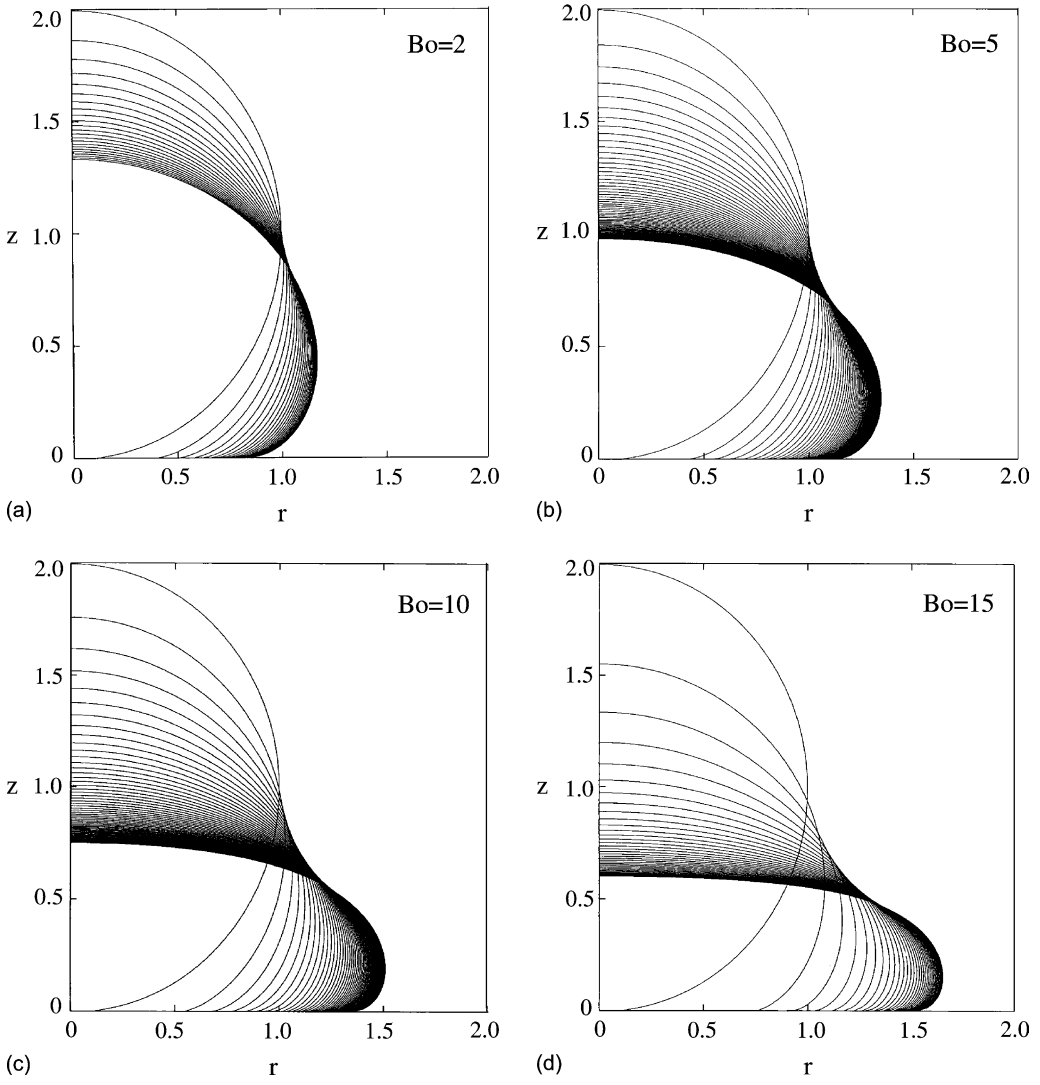

Fig. 4. Time evolution of the drop surface during the transition stage of the process: (a) $Bo = 2$, (b) $Bo = 5$, (c) $Bo = 10$, and (d) $Bo = 15$, and the time step between the curves is: (a), (d)—$\triangle t = 0.05$; (b), (c)—$\triangle t = 0.025$. The time intervals covered are: $0 \leqslant t \leqslant 0.97$ for (a), $0 \leqslant t \leqslant 0.9$ for (b), $0 \leqslant t \leqslant 1.09$ for (c), and $0 \leqslant t \leqslant 1.02$ for (d).

the method of matched asymptotic expansions. For small contact angles the expansions of the solutions in Ca in the outer bulk region and in the immediate vicinity of the CL were matched in Hocking and Rivers (1982) in an intermediate region of size $\epsilon = -1/\ln\lambda$. The dependence of Ca on α (α being the apparent contact angle) was then obtained as the matching condition.

What we seek, however, is the law of the CL motion for arbitrary contact angles. The problem is solved via the perturbation method similar to the one proposed in Cox (1986), and Hocking and Rivers (1982) for small values of Ca. Consider first the outer bulk region and resolve the pressure in two terms as per

$$p = -Bo(z - z_a) + \tilde{p}. \tag{29}$$

Then it follows from (18) that

$$\nabla\tilde{p} = \triangle\mathbf{u}. \tag{30}$$

The normal stress balance in the new variables can be written as

$$\tilde{f}_{\mathrm{n}} = \kappa - Bo(z - z_a), \quad r = h(z,t). \tag{31}$$

The condition of vanishing of the tangential stress (20) conserves its form in the new variables. Since the capillary number is assumed to be small, we expand the unknown variables in Ca as per

$$h = h_0 + Cah_1 + \cdots, \quad \beta = \beta_0 + Ca\beta_1 + \cdots, \tag{32}$$

$$\tilde{f}_{\mathrm{n}} = -c + Ca\tilde{f}_{\mathrm{n}}^{1} + \cdots, \quad \mathbf{u} = Ca\mathbf{u}_1 + \cdots, \tag{33}$$

where $c(t)$ is an unknown function (the modified pressure $\tilde{p}$ should be constant in the zeroth order in Ca).

In the zeroth order in Ca, we obtain from (31), (10) and (32) the following set of equations for determination of the drop generatrix:

$$\frac{\partial h_0}{\partial s} = \cos\beta_0, \tag{34}$$

$$\frac{\partial z}{\partial s} = \sin\beta_0, \tag{35}$$

$$\frac{\partial \beta_0}{\partial s} = c + Bo(z - z_a) - \frac{\sin\beta_0}{h_0}. \tag{36}$$

with the conditions

$$h_0(0,t) = 0, \quad z(0,t) = z_a, \quad \beta_0(0,t) = 0, \quad z(s_{\mathrm{CL}},t) = 0. \tag{37}$$

The condition of volume conservation should also be added. It has the form (see (22))

$$\int_0^{s_{CL}} h_0 z\cos(\beta_0)\,\mathrm{d}s = \frac{2}{3}. \tag{38}$$

From (34)–(38) we can find the drop generatrix in the form $h = h_0(z, z_a(t))$ and the apparent contact angle $\alpha(z_a)$ and CL coordinate $a(z_a)$ can be found as per

$$\alpha = -\beta(s_{\mathrm{CL}},t), \quad a = h_0(s_{\mathrm{CL}},t), \tag{39}$$

for any fixed apex coordinate z_a.

Therefore we can write

$$\frac{\partial h_0}{\partial t} = CaF(z, z_a(t)), \tag{40}$$

where the function $F(z, z_a(t)) = (\partial h_0/\partial z_a)/(\partial a/\partial z_a)$ can be found numerically.

Note that the kinematic boundary condition (7) can be rewritten as

$$u_{\mathrm{n}} = \mathbf{u}\cdot\mathbf{n} = u_z\cos\beta - u_r\sin\beta = -\frac{\partial h}{\partial t}\sin\beta. \tag{41}$$

Substituting (40) in (41), we obtain

$$u_{\mathrm{n}}^{1} = -F(z, z_a(t)) \sin \beta_0, \tag{42}$$

where u_{n}^{1} is the normal velocity component at the drop surface in the first order in Ca. The latter is used as the boundary condition for (30), generating a non-zero solution in the domain bounded by the drop generatrix $h_0(z, z_a)$. The second boundary condition at the drop surface is given by (8). In the outer region we can neglect the slip term in (6) and use (5) as the boundary condition at the plane $z = 0$. These conditions are used for solving the Stokes equations uniquely, and we can determine the value of $\tilde{f}_{\mathrm{n}}^{1}$ on the drop surface described by the function h_0. The condition for the normal stresses (31) containing $\tilde{f}_{\mathrm{n}}$ should then be used for the correction to the shape of the drop generatrix in the first order in Ca, which is necessary for finding the expansions near the CL.

In the present case the Stokes equations with the boundary conditions are unsolvable analytically, unlike the situation in Hocking and Rivers (1982) for the case $Bo = 0$ corresponding to a circular drop surface. Accordingly, we are searching for numerical solution using the BEM, details of whose implementation for solving Eq. (30) can be found in Becker (1992), Pozrikidis (1992), van de Vorst (1994). It is well known that the vorticity and stresses are singular at the CL. Moreover, they contain very steep gradients near the CL, and very fine resolution of the free surface is needed there. This difficulty can be obviated through the following consideration. Let

$$\mathbf{u}_{\mathrm{l}} = \mathbf{u}_{\mathrm{H}} + \hat{\mathbf{u}}, \tag{43}$$

$$\tilde{\mathbf{f}}_{\mathrm{l}} = \tilde{\mathbf{f}}_{\mathrm{H}} + \hat{\mathbf{f}}, \tag{44}$$

$\mathbf{u}_{\mathrm{H}}$ and $\tilde{\mathbf{f}}_{\mathrm{H}}$ being the analytical solutions of Hocking and Rivers (1982) for a circular drop with the same axis of symmetry, contact angle α and CL position a and unit CL velocity. In the region near the CL this solution has the form of the Moffatt solution for a two-dimensional wedge (Moffatt, 1964)

$$u_x^{\mathrm{H}} = \frac{\sin \alpha}{\alpha - \sin \alpha \cos \alpha} (\phi_{\mathrm{l}} \sin \alpha + \cos \phi_{\mathrm{l}} \cos(\phi_{\mathrm{l}} - \alpha) - \cos \alpha), \quad r_{\mathrm{l}} \to 0. \tag{45}$$

$$u_y^{\mathrm{H}} = \frac{\sin \alpha}{\alpha - \sin \alpha \cos \alpha} (\phi_{\mathrm{l}} \cos \alpha - \sin \phi_{\mathrm{l}} \cos(\phi_{\mathrm{l}} - \alpha)), \quad r_{\mathrm{l}} \to 0, \tag{46}$$

where ϕ_{l} is the polar angle determining the position of a surface point relative to the CL, r_{l} is the distance from the CL to a surface point (see Fig. 1). Note that it is actually assumed that the effect of the curvature of the CL on the flow in its vicinity is negligibly small, and the Moffatt solution is still valid approximately in the axisymmetric case. Note also that Voinov (1976, 1978) employed previously the Moffatt solution to derive an expression for the dependence of α on Ca.

The normal stress component in the vicinity of the CL is given by

$$\widetilde{\mathbf{f}}_{\mathrm{H}} \cdot \mathbf{n} = \frac{2 \sin \alpha}{(\alpha - \sin \alpha \cos \alpha) r_{\mathrm{l}}}, \quad r_{\mathrm{l}} \to 0. \tag{47}$$

Expressions (45)–(47) yield an analytical representation of the singularity at the CL. Thus all we have to do, using BEM, is to find the correction terms $\hat{\mathbf{u}}$, $\hat{\mathbf{f}}$, satisfying the following boundary conditions on the surface:

$$\hat{\mathbf{u}} \cdot \mathbf{n} = u_{\mathrm{n}}^{1} - \mathbf{u}_{\mathrm{H}} \cdot \mathbf{n}, \quad r = h_0(z, z_a), \tag{48}$$

$$\hat{\mathbf{f}} \cdot \boldsymbol{\tau} = -\tilde{\mathbf{f}}_{\mathrm{H}} \cdot \boldsymbol{\tau}, \quad r = h_0(z, z_a). \tag{49}$$

From (48) and (49) and the fact that $\widetilde{\mathbf{f}}_{\mathrm{H}} \cdot \boldsymbol{\tau} = 0$ on the surface corresponding to a circular generatrix, it follows that $\hat{\mathbf{u}} \cdot \mathbf{n} \to 0$, $\hat{\mathbf{f}} \cdot \boldsymbol{\tau} \to \text{const}$ if $r_1 \to 0$. Then there is no need for numerical processing of the steep gradients associated with the singularity.

The correction to the surface shape at the first order in Ca, h_1 and β_1, can be found from the normal stress balance (31). Substitution of (32) in (31), using (34)–(37) yields the following set of equations:

$$\frac{\partial \beta_1}{\partial s} = \frac{\sin \beta_0(s)}{h_0^2(s)} h_1 - \cot \beta_0(s)(c + Bo(z(s) - z_a))\beta_1 + \tilde{f}_{\mathrm{n}}^1(s) + \tilde{c}, \tag{50}$$

$$\frac{\partial h_1}{\partial s} = -\frac{\beta_1}{\sin \beta_0(s)}. \tag{51}$$

with the conditions at the apex

$$\beta_1 = 0, \quad h_1 = 0, \quad \text{at } s = 0. \tag{52}$$

Here $z(s)$, $\beta_0(s)$, $h_0(s)$ are the functions found from (34)–(37) and s has the same meaning as in (34)–(37). To avoid numerical difficulties in (50) and (51), stemming from the fact that $\beta_0(0) = 0$, $h_0(0) = 0$, we replace (52) by the conditions at $s = \epsilon_{\mathrm{s}} \ll 1$. By (50) and (51) these conditions take the form

$$h_1(\epsilon_{\mathrm{s}}) = -\frac{\tilde{c}\epsilon_{\mathrm{s}}}{2c}, \quad \beta_1(\epsilon_{\mathrm{s}}) = \frac{\tilde{c}\epsilon_{\mathrm{s}}}{4}. \tag{53}$$

The function $\tilde{c}$ can be found numerically from the condition of volume conservation (22). Using (51) we obtain that, in the first order in Ca, this condition can be expressed as per

$$\int_0^{s_{CL}} h_1 h_0 \sin \beta_0 \, \mathrm{d}s = 0. \tag{54}$$

For matching with the inner region of molecular size near the CL, where slip takes place, we need to find the asymptotic value of β_1 there. Substituting (47) in (50), we derive (for better convenience of the matching procedure) the negative counterpart of β, denoted δ

$$\delta \to \alpha + Ca\left[\frac{2\sin\alpha}{\alpha - \sin\alpha\cos\alpha} \ln r_1 + \overline{Q}_0(\alpha, Bo)\right] + \mathrm{O}(Ca^2), \quad r_1 \to 0, \tag{55}$$

where $\overline{Q}_0$ is a constant obtainable from the numerical solution.

The asymptotic of the solution, satisfying the boundary condition (14) in the inner region of size λ, is according to Cox (1986), Hocking and Rivers (1982)

$$\delta \to \alpha_{\mathrm{s}} + Ca\left[\frac{2\sin\alpha_{\mathrm{s}}}{\alpha_{\mathrm{s}} - \sin\alpha_{\mathrm{s}}\cos\alpha_{\mathrm{s}}} (\ln \tilde{r} + 1) + \overline{Q}_i(\alpha_{\mathrm{s}})\right] + \mathrm{O}(Ca^2), \quad \tilde{r} \to 0, \tag{56}$$

where $\tilde{r} = r_1/\lambda$.

The expansions (55) and (56) are matched as in Hocking and Rivers (1982) via consideration of an intermediate region of size $\epsilon = -1/\ln\lambda$. In this region the solution of the Stokes equation does not depend on the entire geometry. It has, up to $\mathrm{O}(\epsilon^2)$, the form of the analytical solution of

Moffatt, which refers to a plane boundary. In the present case the drop boundary is curved, but its characteristic radius of curvature is much larger than λ, as is also that of the CL. The normal stress balance in the intermediate region then reads (Cox, 1986)

$$\frac{\mathrm{d}\delta}{\mathrm{d}\tilde{r}} = \frac{Ca}{\tilde{r}} \frac{2\sin\delta}{\delta - \sin\delta\cos\delta} + \mathrm{O}(\epsilon^3). \tag{57}$$

In Somalinga and Bose (2000), this solution was verified by direct numerical simulations for $Ca \ll 1$. The matching procedure thus described in brief, yields the following dependence:

$$Ca(\alpha, Bo, \alpha_s) = \frac{1}{2} \frac{G(\alpha) - G(\alpha_s)}{\epsilon^{-1} + Q_i(\alpha_s) - Q_0(\alpha, Bo)} + \mathrm{O}(\epsilon^3), \tag{58}$$

where

$$G(\alpha) = \int_0^\alpha \frac{t - \sin(t)\cos(t)}{\sin(t)}\,\mathrm{d}t, \tag{59}$$

$$Q_0(\alpha, Bo) = G'(\alpha)\overline{Q}_0(\alpha, Bo) - 1, \quad Q_i(\alpha_s) = G'(\alpha_s)\overline{Q}_i(\alpha_s), \tag{60}$$

and the primes denote differentiation.

The term $Q_i(\alpha_s)$ is determined by the processes in the vicinity of the CL (such as the disjoining pressure resulting from the van der Waals forces) and does not depend on the external flow. In Hocking and Rivers (1982) it was calculated using the slip boundary condition (6). Therefore, the only term we need in (58) to calculate Ca for a particular α (or a) is Q_0, which is obtainable numerically by BEM. This was done in the present work for the range of angles $\alpha_s < \alpha < \pi - 0$, and Bond numbers $2 \leqslant Bo \leqslant 15$. For the moderate Bond numbers BEM was used to find a solution of a sub-problem needed in the asymptotic analysis. Namely, it was used to calculate the term $\tilde{f}_n^1(s)$ entering Eq. (50). To do that, Eq. (30) was solved by BEM with the boundary conditions (5), (8) and (42). Then Q_0 could be found from the system (50) and (51) as $s \to s_{CL}$.

Note that in the present work we assume that drops spread over a plain wall. Surface roughness is known to decrease (increase) α at a given Ca, if $\alpha < \pi/2$ ($\alpha > \pi/2$) (Dussan, 1979).

4.4. Wetting stage: results

Consider now the results for the wettability stage at $t \geqslant t_*$. At the moment $t = t_*$ the rate of the CL propagation becomes equal to that which would result from the molecular wettability effects affected by the bulk flow. At $t > t_*$ the motion of the CL is driven mainly by the wettability effects, albeit there still is sufficiently strong bulk flow due to gravity. The drop evolution at $t \geqslant t_*$ is illustrated in Fig. 5(a)–(d), where the calculated drop shapes given by (34)–(38) for different values of the apex height z_a (equivalent to different values of time) and $Bo = 2$–15 are shown. The dependences $Ca(\alpha)$ corresponding to these values of Bo are plotted in Fig. 6 for the value $\epsilon = 0.01$ and $\alpha_s = 0.3$. The dashed–dotted curve 6 in Fig. 6 corresponds to the universal law (Cox, 1986)

$$Ca(\alpha) = \frac{\epsilon}{2}(G(\alpha) - G(\alpha_s)). \tag{61}$$

The results in Fig. 6 actually show that the stronger the bulk flow at higher values of the Bond number, the larger the deviations from the universal Hoffman relation (61). The apparent contact

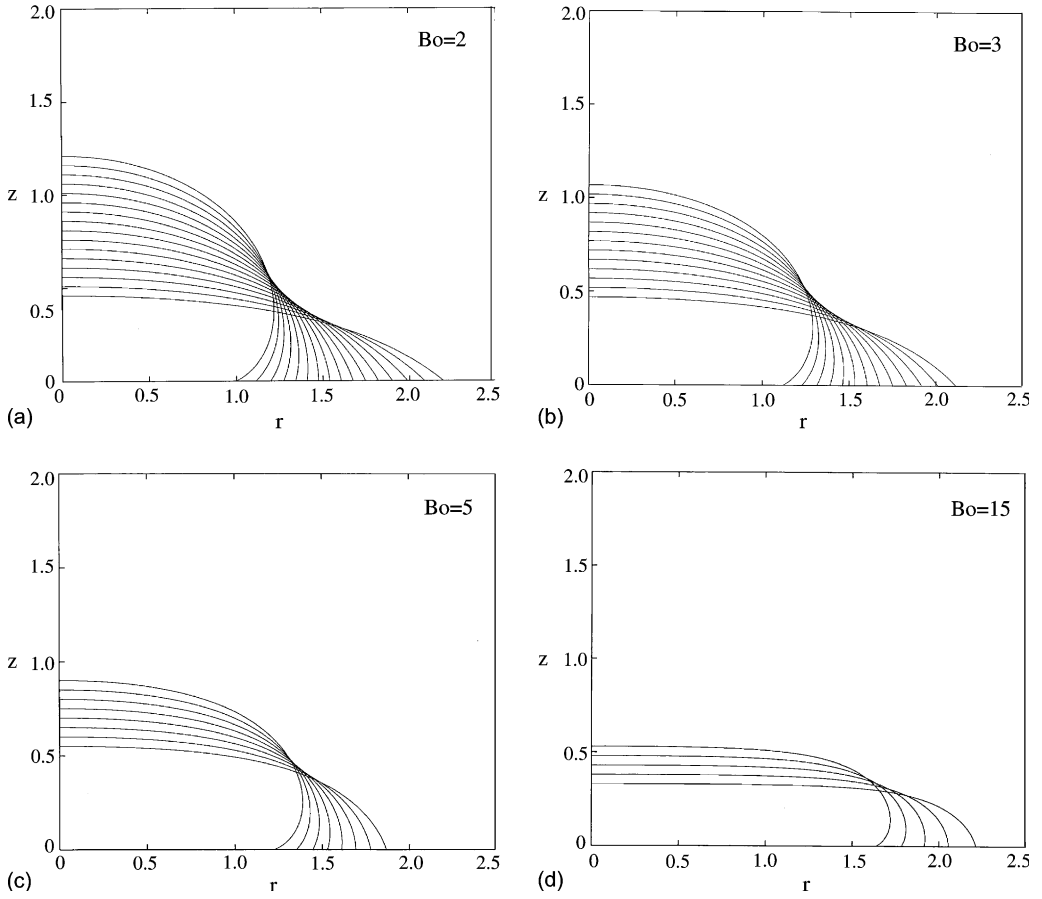

Fig. 5. Evolution of the drop shape at the wetting stage for moderate values of the Bond number: (a) $Bo = 2$, (b) $Bo = 3$, (c) $Bo = 5$, (d) $Bo = 15$. The initial drop configuration corresponds to the apparent contact angle $\alpha \sim 3$, and the apex height step between the curves is $\delta z_a = 0.05$, which is equivalent to time stepping.

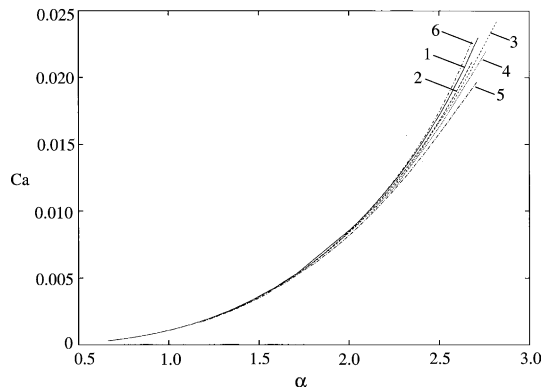

Fig. 6. Dependence of the capillary number Ca on the apparent contact angle α. Curve 1 corresponds to $Bo = 2$; 2—$Bo = 5$; 3—$Bo = 7$; 4—$Bo = 9$; 5—$Bo = 15$. Curve 6 corresponds to the universal Hoffman relation (61).

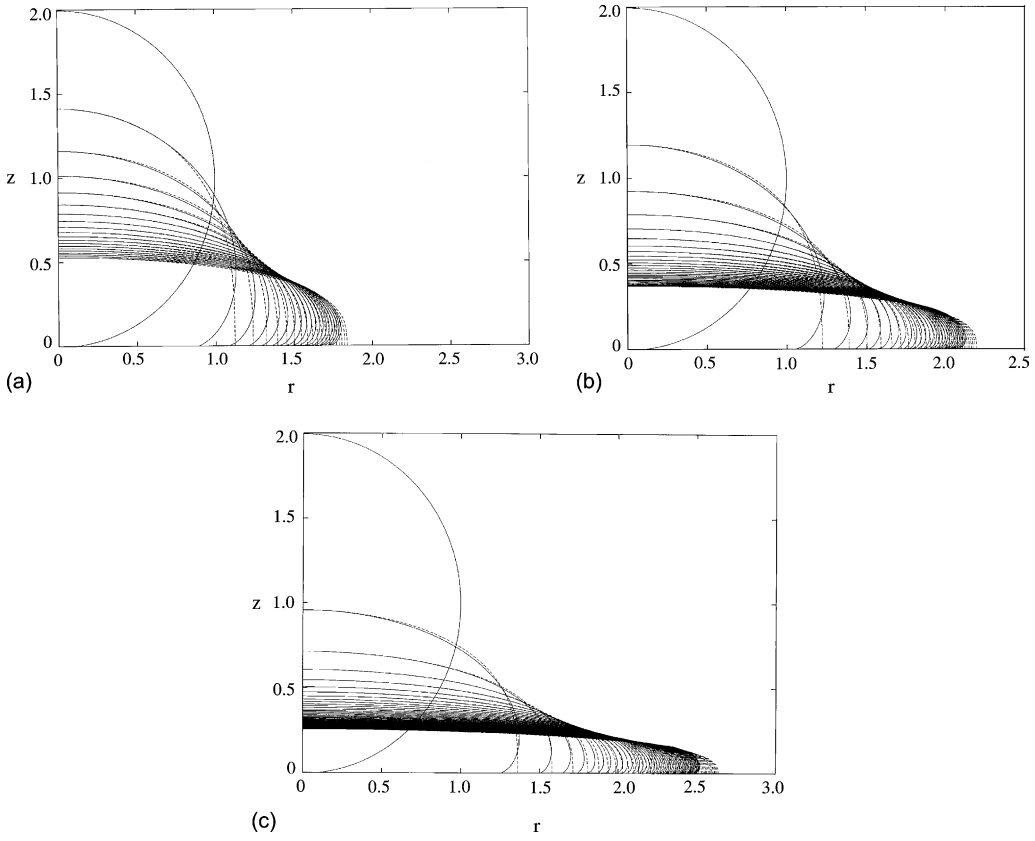

Fig. 7. Time evolution of the drop surface at high values of the Bond number. The initial drop configuration corresponds to $t = 0$, (a) $Bo = 50$, (b) $Bo = 100$, (c) $Bo = 200$, and the time step between the curves is: $\triangle t = 0.025$. The dashed curves correspond to (64) with the same apex heights as those obtained numerically. The time intervals covered are: $0 \leqslant t \leqslant 0.47$ for (a), $0 \leqslant t \leqslant 0.695$ for (b), $0 \leqslant t \leqslant 2.025$ for (c).

angle α is significantly affected by the bulk flow at higher values of the Bond number, increasing as the latter increases at a constant Ca. This result is fully consistent with the observations in the experiments of Ngan and Dussan (1982), which show an increasing effect of the strong bulk flow forcing on α (cf. Fig. 7 there).

As time increases, the contact angle α becomes small and the gravity/bulk flow effects become less significant for sufficiently thin drops, and all the curves in Fig. 6 merge. The drops then spread in accordance with the well-known Hoffman relation. Only for $Bo = 0$ is the dependence $Ca(\alpha)$ sufficiently close to the universal law (61) throughout the whole range of variation of the apparent angle.

From Fig. 6 it follows that the capillary number is relatively small over a wide range of apparent contact angle variation: e.g. $Ca \leqslant 0.025$ for $\alpha \leqslant 3$ ($\alpha \leqslant 172°$). The method of asymptotic expansions is thus applicable for the most of the contact angles. The value of Ca decreases as the Bond number increases at a fixed value of α. Note that the asymptotic expansion used is valid only if the condition

$$\epsilon|Q_0| \ll 1 \tag{62}$$

is satisfied, and Fig. 6 shows that this cannot be the case for large values of *Bo* and values of α close to π. The solution then fails due to the following reasons. For sufficiently large Bond numbers the gravity forcing, dominant in the outer region, plays also an important role in the intermediate region of the order of ϵ, in which case correct matching in the latter is impracticable. On the other hand, for small values of the apparent contact angle the gravity force affects a distance of the order of $\sim 1/\sqrt{Bo}$ from the CL (Hocking, 1983). Therefore, if the condition

$$\frac{1}{\sqrt{Bo}} \gg \epsilon \tag{63}$$

is satisfied, the gravity effects do not play any role in the intermediate region and matching is possible. Accordingly, for moderate values of *Bo* the motion of the CL is close to the predictions of the Hoffman's relation. Fig. 6 shows that for α close to π the gravity effects can be significant already at $Bo \sim 1$.

4.5. The overall picture at moderate Bond numbers

The overall picture of drop spreading for moderate Bond numbers revealed by the calculations is as follows. An initially circular drop deforms under the action of gravity and capillarity, while the molecular van der Waals effects do not play any role. At this stage the CL moves at a rate depending on the parameters σ, μ, ρ, g and time only. At the CL rolling motion sets in and the apparent contact angle equals π at this stage of motion. As the drop surface tends to the shape described by (34)–(38) still with $\alpha = \pi$ (see Fig. 4(a)–(d)), the CL motion rate reduces to the order $O(\epsilon)$. In parallel the molecular van der Waals effects become significant. From then on, not only the bulk parameters α, μ, ρ and g are of importance, but also the molecular one, $\bar{\lambda}$ (or $\epsilon = -1/\ln(\bar{\lambda}/a_0)$ in the dimensionless form). At this stage the apparent contact angle α gradually decreases from π to its stationary value α_s (cf. Fig. 5). This evolution of the apparent contact angle follows the universal Hoffman's law (61) and is relatively slightly affected by the effects of the bulk flow. Deviations from (61) are of importance only close to $\alpha = \pi$, where the perturbation theory is inapplicable.

5. Large Bond numbers

For large Bond numbers gravity dominates capillarity in the most of the drop body, except for a region of scale $1/\sqrt{Bo}$ near the circumferential rim (Hocking, 1983). When the drop is flattened, the lubrication arguments become applicable. A similarity solution for this case was obtained by this approach in Hocking (1983); see also Huppert (1982). In the dimensionless variables used here, it has the following form:

$$z = \frac{A}{a^2}\left(1 - \left(\frac{r}{a}\right)^2\right)^{1/3}, \quad |r| \leqslant a, \tag{64}$$

$$a^7 \frac{da}{dt} = \frac{2BoA^3}{9}, \tag{65}$$

where the constant $A = 16/9$.

The lubrication approximation is inapplicable near the circumferential rim, where (64) yields a slope angle equal to $\pi/2$, and the capillary effects are significant. In Hocking (1983) it was shown that the solution (64) can be matched with that in the inner region near the rim, of the order of $1/\sqrt{Bo}$, and the CL motion can be described using (65), except for the stage of evolution where $\alpha \to \alpha_s$ and the drop surface approaches its equilibrium shape. In the present case the lubrication approximation is inapplicable at the initial stage of the evolution when the drop is almost circular, but it was tentatively assumed that the similarity solution becomes realizable after a larger time interval. To verify this assumption, numerical calculations were done for $Bo = 50$, 100 and 200. In this case the numerical procedure for the initial transition stage followed the one described in subsection 4.2. Also, as it was explained in the preceding section, in the case of large Bond numbers the method of matching asymptotic expansions, used for $Bo \leqslant 15$, is impracticable. Expressions (58)–(60) are incorrect for any value of α except those tending to α_s. Therefore in the present work the wetting stage was not considered in the case of large Bond numbers. This stage, however, would correspond to extremely squeezed shapes when the whole meaning of the contact angle becomes problematic.

The evolution of the drop generatrix in time, obtained numerically for $Bo = 50$, 100 and 200 for the transition stage $0 \leqslant t \leqslant t_*$, which is very long for those values of Bo, is shown in Fig. 7(a)–(c). The dashed curves correspond to (64) with the same apex heights as those obtained numerically. It is seen that Eq. (64) agrees closely with the numerical results for most of the drop generatrix over a certain time interval, when the drop has already been sufficiently flattened. (A similar agreement between (64) and (65) and the experimental data was found in Marino et al., 1996).

After that, when the wetting effects become important, the agreement disappears. At the transition stage of Fig. 7, rolling motion of the CL is realized. When its rate becomes equal to that due to the wetting effects, a switch is in order as discussed in Section 4. It is emphasized that the solution (64) and (65) remains valid even at the wettability stage (where the gravity effects are still important). The latter has been proved in Hocking (1983), where (64) was matched with the solution in the inner region.

Experiments of Marino et al. (1996) suggest that the shapes of the leading head of spreading drops virtually remain almost self-similar as long as the rolling motion persists at the CL (an intermediate quasi-self-similarity). To verify this hypothesis, we used the data corresponding to Fig. 7(b) ($Bo = 100$). The shapes of the drop head at different time moments were replotted in Fig. 8 in the coordinates $(r - a)/(r_{max} - a)$ and $z/(r_{max} - a)$. The results show that, indeed, this re-scaling virtually allows collapse of all the curves onto a single one. Moreover, in Fig. 8 we also plotted the cumulative experimental date from Fig. 12 of Marino et al. (1996) for an almost self-similar head of a polydimethylsiloxane drop of radius $a_0 = 7.11$ cm, $\rho = 0.96$ g/cm^3, $\mu = 1223.7$ g/(cm s) and $\sigma = 21$ g/s^2. In Fig. 8 it is clearly seen that the data agree with the present numerically generated shapes. This suggests that the almost self-similar head shape of rolling drops is also invariant in respect to the variation of the Bond number.

The CL motion rate, shown as the capillary number Ca as a function of position a obtained numerically, is demonstrated in Fig. 9 for $Bo = 50$, 100 and 200 for the transition stage $0 \leqslant t \leqslant t_*$.

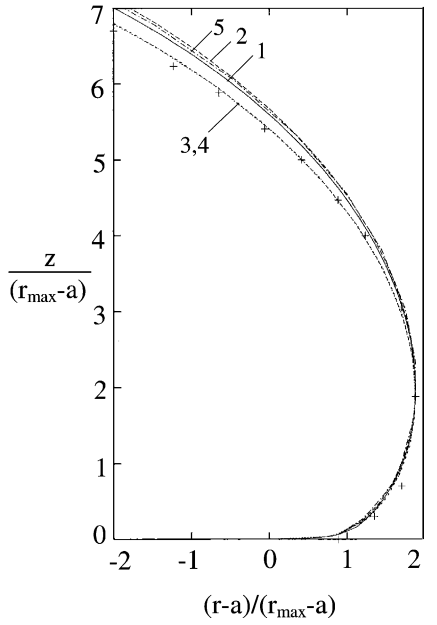

Fig. 8. Quasi-self-similarity of the leading head of the drop with rolling motion at the CL. $Bo = 100$ (corresponds to Fig. 7(b)). To curve 1 corresponds $t = 0.045$; 2—$t = 0.07$; 3—$t = 0.095$; 4—$t = 0.17$; 5—$t = 0.23$. The curves show the results of the present calculations. The cumulative experimental data of Marino et al. (1996) are shown by symbols.

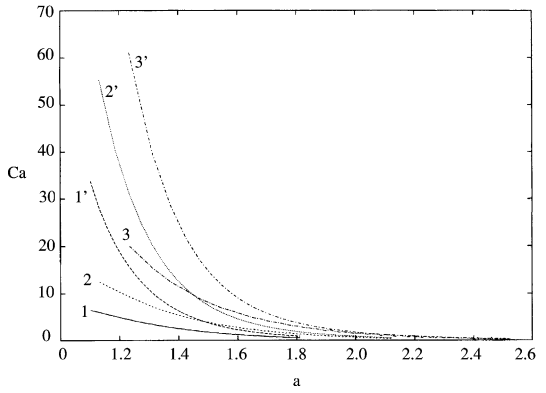

Fig. 9. Capillary number based on the motion rate of the CL as a function of its position at high values of the Bond number. 1—$Bo = 50$, 2—$Bo = 100$, 3—$Bo = 200$. Curves 1′, 2′ and 3′, corresponding to the above values of the Bond number, were plotted using the analytical solution (64) and (65).

The corresponding dependences (64) and (65) are also plotted. It is seen that if the drop shapes are close to those of (64) (cf. Fig. 7), which corresponds to $1.6 \leqslant a \leqslant 1.75$ for curves 1 and 1′, to $1.8 \leqslant a \leqslant 2.1$ for curves 2 and 2′, and to $1.9 \leqslant a \leqslant 2.4$ for curves 3 and 3′ in Fig. 9, the numerical and analytical results shown in Fig. 9 agree.

6. Summary

In the case of spreading of an axisymmetric drop on a horizontal wall the following scenario was revealed by the modeling of the present work. After an almost instantaneous stage, when the drop surface evolves from a pointwise to a small but finite contact area, a transition stage begins. The latter is almost completely governed by the effect of gravity-driven bulk flow. As a result, rolling motion sets in at the CL. The duration of this stage lengthens as the Bond number increases. During the transition stage the motion rate of the contact line (normalized as the capillary number) decreases as the drop spreads. At its end the capillary number achieves the level characteristic of the wetting effects. During the next stage of spreading the dependence of the apparent contact angle on the capillary number begins to approach the Cox relation (61), but the gravity-driven bulk flow evidently affects that angle even at this stage; the angle is larger for the larger Bond number (gravity forcing). At the end of this stage the wetting effects become dominant and universal Hoffman relation comes into play.

Acknowledgements

This research was partially supported by GIF—the German–Israeli Foundation for Scientific Research and Development, Research Grant no. I-536-097.14/97. S.N. Reznik acknowledges support by the Center for Absorption in Science, Ministry of Immigrant Absorption (State of Israel).

References

Becker, A.A., 1992. The Boundary Element Method in Engineering. A Complete Course. McGraw-Hill, New York.

Betelu, S., Diez, J., Thomas, L., Gratton, R., Marino, B., 1997. A boundary element method for viscous gravity currents. Int. J. Numer. Meth. Fluids 25, 1–19.

Blake, T.D., 1993. Dynamic contact angles and wetting kinetics. In: Berg, J.C. (Ed.), Wettability. Marcel Dekker, New York, pp. 251–309.

Chandra, S., Avedisian, C.T., 1991. On the collision of a droplet with a solid surface. Proc. R. Soc. Lond. A 432, 13–41.

Chen, Q., Rame, E., Garoff, S., 1996. Experimental studies on the parametrization of liquid spreading and dynamic contact angles. Colloid. Surface. A: Physicochem. Eng. Aspect 116, 115–124.

Cox, R.G., 1986. The dynamics of the spreading of liquids on a solid surface. Part 1. Viscous flow. J. Fluid Mech. 168, 169–194.

Davidson, M.D., 2000. Boundary integral prediction of the spreading of an inviscid drop impacting on a solid surface. Chem. Eng. Sci. 55, 1159–1170.

de Gennes, P.G., 1985. Wetting: statics and dynamics. Rev. Mod. Phys. 57, 827–863.

de Gennes, P.G., Hua, X., Levinson, P., 1990. Dynamics of wetting: local contact angles. J. Fluid Mech. 212, 55–63.

Dussan V, E.B., 1979. On the spreading of liquids on solid surfaces: static and dynamic contact lines. Ann. Rev. Fluid Mech. 11, 371–400.

Dussan V, E.B., Davis, S.H., 1974. On the motion of a fluid-fluid interface along a solid surface. J. Fluid Mech. 65, 71–95.

Fermigier, M., Jenffer, P., 1991. An experimental investigation on the dynamic contact angle in liquid–liquid systems. J. Colloid Interf. Sci. 146, 226–241.

Fukai, J., Shiiba, Y., Yamamoto, T., Miyatake, O., Poulikakos, D., Megaridis, C.M., Zhao, Z., 1995. Wetting effects on the spreading of a liquid droplet colliding with a flat surface: experiments and modeling. Phys. Fluids A 7, 236–247.

Fukai, J., Zhao, Z., Poulikakos, D., Megaridis, C.M., Miyatake, O., 1993. Modeling of the deformation of a liquid droplet impinging upon a flat surface. Phys. Fluids A 5, 2588–2599.

Gao, F.Q., Sonin, A.A., 1994. Precise deposition of molten microdrops: the physics of digital microfabrication. Proc. R. Soc. Lond. A 444, 533–554.

Gueyffier, D., Zaleski, S., 1998. Finger formation during droplet impact on a liquid film. Compt. Rend. Acad. Sci. IIB 326, 839–844.

Hatta, N., Fuijmoto, H., Takuda, H., 1995. Deformation process of a water droplet impinging on a solid surface. Trans. ASME: J. Fluid Eng. 117, 394–401.

Hayes, R.A., Ralston, J., 1993. Forced liquid movement on low energy surfaces. J. Colloid Interf. Sci. 159, 429–438.

Hocking, L.M., 1983. The spreading of a thin drop by gravity and capillarity. Q. J. Mech. Appl. Math. 36, 55–69.

Hocking, L.M., Rivers, A.D., 1982. The spreading of a drop by capillary action. J. Fluid Mech. 121, 425–442.

Hoffman, R., 1975. A study of the advancing interface. I. Interface shape in liquid–gas systems. J. Colloid Interf. Sci. 50, 228–241.

Huppert, H.E., 1982. The propagation of two-dimensional and axisymmetric viscous gravity currents over a rigid horizontal surface. J. Fluid Mech. 121, 43–58.

Marino, B.M., Thomas, L.P., Diez, J.A., Gratton, R., 1996. Capillary effects on viscous gravity spreadings of wetted liquids. J. Colloid Interf. Sci. 177, 14–30.

Moffatt, H.K., 1964. Viscous and resistive eddies near a sharp corner. J. Fluid Mech. 18, 1–18.

Ngan, C.G., Dussan V, E.B., 1982. On the nature of the dynamic contact angle: an experimental study. J. Fluid Mech. 118, 27–40.

Pasandideh-Fard, M., Qiao, Y.M., Chandra, S., Mostaghimi, J., 1996. Capillary effects during droplet impact on a solid surface. Phys. Fluids 8, 650–659.

Pozrikidis, C., 1992. Boundary Integral and Singularity Methods for Linearized Viscous Flow. Cambridge University Press, Cambridge.

Reznik, S.N., Yarin, A.L., 2002. Spreading of a viscous drop due to gravity and capillarity on a horizontal or an inclined dry wall. Phys. Fluids 14, 118–132.

Rieber, M., Frohm, A., 1999. A numerical study on the mechanism of splashing. Int. J. Heat Fluid Flow 20, 455–461.

Schiaffino, S., Sonin, A.A., 1997a. Formation and stability of liquid and molten beads on a solid surface. J. Fluid Mech. 343, 95–110.

Schiaffino, S., Sonin, A.A., 1997b. Motion and arrest of a molten contact line on a cold surface: an experimental study. Phys. Fluids 9, 2217–2226.

Somalinga, S., Bose, A., 2000. Numerical investigation of boundary conditions for moving contact line problems. Phys. Fluids 12, 499–510.

Thompson, P.A., Robbins, M.O., 1989. Simulations of contact-line motion: slip and the dynamic contact angle. Phys. Rev. Lett. 63, 766–769.

van de Vorst, G.A.L., 1994. PhD Thesis. Modeling and numerical simulation of viscous sintering. Eindhoven University of Technology, The Netherlands.

Voinov, O.V., 1976. Hydrodynamics of wetting. Fluid Dyn. 11, 714–721.

Voinov, O.V., 1978. Asymptotics of the free surface of viscous fluid in creeping flow and a dependence of the contact angle on the velocity. Sov. Phys. Dokl. (English translation) 23, 891–893.

Waldvogel, J.M., Poulikakos, D., 1997. Solidification phenomena in picoliter size solder droplet deposition on a composite substrate. Int. J. Heat Mass Transfer 40, 295–309.

Weiss, D.A., Yarin, A.L., 1999. Single drop impact onto liquid films: neck distortion, jetting, tiny bubble entrainment, and crown formation. J. Fluid Mech. 385, 229–254.

Yarin, A.L., Weiss, D.A., 1995. Impact of drops on solid surfaces: self-similar capillary waves, and splashing as a new type of kinematic discontinuity. J. Fluid Mech. 283, 141–173.

Zhou, M.Y., Sheng, P., 1990. Dynamics of immiscible-fluid displacement in a capillary tube. Phys. Rev. Lett. 64, 882–885.